#14A Dupl PUB-74-152-E E-0014 #14A PRL

Small Momentum Transfer p-p Inelastic Scattering at 300 GeV/c *

S. CHILDRESS, P. FRANZINI

Columbia University, New York, N.Y.

J. LEE-FRANZINI, R. McCARTHY, R.D. SCHAMBERGER, Jr.

SUNY at Stony Brook, Stony Brook, N.Y.

---

* Research supported in part by the National Science Foundation.

ABSTRACT

We have performed an experiment on p-p inelastic scattering at National Accelerator Laboratory to study the reaction $p + p \rightarrow p + X$. We cover the range in $|t|$ from 0.019 to 0.19 $(GeV/c)^2$ by measuring the low energy recoiling protons. The range in M_X^2 measured is from 0 to 60 GeV^2. The "diffractive" cross section is determined to be in the range $3.2 < \sigma < 4.7$ mb. Unexpected behavior is observed at low $|t|$ for $8 < M_X^2 < 14$ GeV^2.

I. INTRODUCTION

The total proton-proton scattering cross section at high energy is almost constant.[1,2] The small rise recently observed appears to be mostly due to a rise of the inelastic cross section.[3] The elastic cross section itself appears to be mostly a shadow of the absorption.[3] It thus appears that the main features of high energy interactions are determined by the inelastic cross section. The bulk of such cross sections is known to be due to low momentum transfer interactions; typically a large fraction of the inelastic cross section has $|t| < 0.2\ (\mathrm{GeV}/c)^2$. It is therefore of great interest to study in detail inelastic scattering in the low t region. Many authors have discussed what might be expected for the process

$$p + p \rightarrow p + X \qquad (1)$$

at small momentum transfer (t). The possibility of inelastic diffraction was pointed out a long time ago by Good and Walker.[4] Inelastic diffraction could have become a major contribution at NAL energies. More recent ideas involve scaling, partons, Regge poles, "multi-Regge" and "triple-Regge" concepts.[5,6,7,8] We have measured the cross section $d^2\sigma/dtdM_X^2$ for reaction (1) using the extracted proton beam at the Neutrino Laboratory at NAL. Data were obtained at 200, 300 and 400 GeV.[9] We report here our results at 300 GeV.

II. EXPERIMENTAL METHOD

The reaction $(p_{in} + p_{target} + p_{recoil} + X)$ is ideally measured at high energy and low $|t|$ by detecting the slow

recoil proton and measuring its kinetic energy T. If we define the square of the four-momentum transfer as $t = q^{\mu} q^{\mu} = (p^{\mu}_{target} - p^{\mu}_{recoil})^2$, then $t = -2m_p T$. Thus, $|t| < 0.2$ $(GeV/c)^2$ corresponds to $T < 100$ MeV. At a given center of mass energy squared, $s \approx 2m_p p_{lab}$ where p_{lab} is the incident proton momentum, reaction (1) is completely determined by only one more Lorentz invariant. This latter is usually chosen to be the total energy of X in its center of mass, i.e., $M_X^2 = (p^{\mu}_{in} + p^{\mu}_{target} - p^{\mu}_{recoil})^2$. In terms of laboratory recoil proton parameters, M_X^2 is given by

$$M_X^2 = m_p^2 + 2pp_{recoil}\cos\theta - 2T(E + m_p) \qquad (2)$$

where θ and p_{recoil} are the lab angle and momentum of the recoil proton, p and E are the beam momentum and energy. M_X^2 ranges between m_p^2 and s.

We use 18 telescopes each consisting of two solid state detectors to identify recoils, measure their kinetic energy and angle. See Fig. 1a. Each telescope covers a lab angle of 0.4° and is separated from the two adjacent ones by $\sim 2.4^{\circ}$. The whole array covers an angular range of $\sim 45^{\circ}$ to $\sim 90^{\circ}$ relative to the beam. The two detectors have thicknesses of 500 μ to 5000 μ. Protons of energy greater than 8 MeV can cross the first detector and protons of energy up to 32 MeV will stop in the second detector. Energies up to 100 MeV can easily be determined by measuring the integrated energy loss in the second counter. The

energy scale for each detector is determined using 5.447 MeV α's. Particles are identified by the correlation between the energies E_1 and E_2 deposited in the two detectors. The rather sophisticated electronics for processing the detector signals has been described elsewhere.[10] We used carbon and polyethene foils of ~ 6.5 mg/cm^2 as targets. Four different targets of each kind were inserted in the beam at slightly different positions along the beam direction. This allowed us to change the angle of each telescope with respect to the beam by increments of about 0.4° thus giving us approximately 60% coverage in the laboratory angle.

The normalization of the carbon and polyethene data is obtained by detecting deuterons and tritons from proton interactions in carbon simultaneously with protons in each telescope. Figure 1b shows the ability of our system to separate such fragments from protons as well as giving a visual indication of their abundance. Such a normalization is performed independently for each telescope. The deadtime of each telescope is continuously measured during each run and is corrected for after the subtraction of carbon data. Further details of this method are given in Ref. 11.

III. DATA COLLECTION AND REDUCTION

A coincidence between the two counters of any telescope represents an event trigger. Upon receipt of a trigger, the amplitudes of all detector signals are stored in sample and hold amplifiers. The information as to which counters had

pulses greater than a preset threshold is also stored, in a set of registers. A scan of the registers causes the appropriate sample and hold amplifiers' outputs to be multiplexed into two 12-bit analog-to-digital converters. Four 16-bit words per event containing the telescope numbers and pulse heights of the two detectors result from these operations. Typically, an event is processed in this way in 12 μs and is entered into a PDP 11 memory in 5 more μs. Up to 4200 events can be entered in memory and written on tape in between accelerator pulses. Our typical event rate ranges between 2000 and 4000 events per pulse with approximately 10^{12} protons on target. The above event rate is mostly determined by the accelerator effective spill length. In order to be able to measure pulse heights to great accuracy an updating deadtime requirement is imposed on each counter. The effective deadtime for each telescope is integrated over each run by counting the instantaneous beam rate (as seen by a scintillation counter telescope pointing at our target) during the time either element of a telescope is turned off. Typically a run corresponds to either a carbon or a polyethene target in one of the four longitudinal positions. Each run lasts approximately 20 minutes and corresponds to half a million triggers. The data discussed here correspond to approximately 10^7 events collected on tape. The analysis of the events is performed off-line on general purpose computers and consists of the following steps:

1. Identify and count deuterons and tritons from carbon and polyethene for each telescope at each of its four angular positions.

2. Reduce for each telescope and angle the two dimensional distributions in the counter signals to a proton kinetic energy distribution.

3. Subtract the normalized carbon distributions from the corresponding polyethene distribution for each telescope and angle.

4. Apply to each run a deadtime correction as measured (this ranges from 1 to 5%).

5. Reduce the T, θ distributions to a t, M_X^2 distribution by calculating the appropriate quantities and jacobian. Then combine the results from all angles and telescopes.

IV. EXPERIMENTAL CHECKS AND CALIBRATION

Before presenting the results we wish to first discuss the checks we have performed on the data. The proper working of each telescope was continuously checked during the run by recording the integrated deadtime and the total number of coincidences. Also the computer gave summaries of the total number of events written on tape for each telescope and the fraction of true coincidence per trigger. This fraction was always larger than 95%. A scatter plot of the two energy signals from the two detectors was displayed on an oscilloscope. A simple visual inspection of plots like that of Fig. 1b is extremely useful to check whether loss

in energy resolution or excessive background suddenly develops due to drift in beam position producing scraping in the beam line elements.

While running with polyethene, recoils from p-p elastic scattering give a bright spot along the proton correlation curve on the scatter plot and their position is strongly correlated with the telescope angle, thus allowing another qualitative check that the proper angles are being covered. The background level at the detectors was monitored by a scintillation telescope parallel to the beam line, placed 1 m away. Another counter was located at the upstream end of the last set of bending magnets approximately 150 ft upstream of our target to monitor the beam entrance into those magnets.

At the event analysis stage, the ratio $H_3:H_2:H$ is computed for each run. A χ^2 comparison to the average allowed us to reject a few records occasionally repeated because of tape drive malfunction. The most conclusive check on the proper working of our spectrometer and on its ability to properly measure $d^2\sigma/dtdM_X^2$ is obtained by a study of elastic p-p scattering. There are 340,000 elastic events contained in the data collected. They are observed in 22 different telescope-angle combinations. The energy values at which the elastics are observed allow us to check both our absolute energy and our absolute angular scales.

Finally the 22 measured cross sections can be perfectly fitted by a simple exponential e^{bt} with a slope parameter $b = 10.7 \pm 0.6\ (\mathrm{GeV/c})^{-2}$ in very good agreement with reported values.[12]

V. RESULTS

In the following, we present our results for the inelastic cross section. It should be noted that we have not performed an absolute measurement of the cross section. However, since we have a very good measurement of the elastic yield, we can use the known values of the elastic cross section to obtain an absolute calibration. We have used the value $\sigma_{el} = 7$ mb.[1] All results following depend on the validity of that number as far as absolute scale is concerned.

Since we have measured the two dimensional function $f(t, M_X^2) = d^2\sigma/dtdM_X^2$, it is somewhat complicated to present all our results. We choose to present some salient features in Figs. 2a and 2b. The first figure gives the invariant cross section $sd^2\sigma/dtdM_X^2$ summed over the entire accepted t range which was $0.019 < |t| < 0.19\ (\mathrm{GeV/c})^2$. The elastic peak has been subtracted in this data by assuming a symmetrical elastic peak and using the values measured below $M_X^2 = m_p^2$. This procedure is justified by the fact that a) the M_X^2 resolution in our data is $\approx \pm 0.55$ GeV^2 at low t and $\approx \pm 1\ \mathrm{GeV}^2$ at high t, b) the elastic peak is perfectly symmetric around its center for approximately three quarters of its height, c) the smearing due to finite

resolution of the inelastic cross section is consistent with our resolution and is amply covered by the statistical error. The elastic peak was subtracted independently for the t regions $0.019 < |t| < 0.094$ and $0.094 < |t| < 0.19$ to properly account for the different M_X^2 resolutions, then the results were combined.

The most striking feature of the cross section is the sudden rise just above threshold, peaking at $M_X^2 \approx 2$ GeV^2, the very fast drop in the region 2 to 16 GeV^2 and the leveling off above M_X^2's of 16 GeV^2. These results are in apparent contrast with similar results obtained at the CERN ISR.[13] A comparison of a part of our data with a typical ISR result is shown in Fig. 2b. (Note that here the cross section presented is $(sd^2\sigma/dtdM_X^2) \times 1/\pi)$. An interesting question is whether the dissimilarity in the results is due to the extreme difference in the t values studied in the two experiments ($\langle t\rangle = -0.056$ vs $\langle t\rangle = -0.35$). While this is certainly possible we feel that it is mostly due to a difference in resolution. The same figure shows our data smeared out by folding the M_X^2 resolution quoted by the CERN CHLM experiment. Note that apart from a vertical shift due to the fast drop with $|t|$ of the cross section, the actual shape is now much more similar.

We now consider the t dependence of the cross section. This seems to vary a great deal with M_X^2 and does show very interesting properties. The peak at $M_X^2 \sim 2$ GeV has a t

dependence of the type e^{bt} with $b = 15 \pm 1$ $(GeV/c)^2$, (statistical error only). Such sharp t dependence in reaction (1) has already been observed at AGS-PS energies.[14] The actual value of the cross section at this M_X^2 appears to remain constant from 10 to 300 GeV. Similar preliminary results have also been reported by the US-USSR collaboration.[15] In the mass squared region from 3 to 6 GeV^2, we obtain slopes around 5 to 6 $(GeV/c)^{-2}$. The most remarkable behavior is however observed in the mass squared region $8 < M_X^2 < 14$ GeV^2, where the cross section appears to decrease for t approaching zero. This effect is shown in Fig. 3. In the same figure, the data for mass squared between 20 and 60 GeV^2 are shown. While the points for that mass region do scatter somewhat, they can be fit with an exponential ($b = 3.4 \pm 1.2$, $\chi^2 = 15$ with 7 degrees of freedom).

VI. DISCUSSION

It is customary to attempt to extract from this kind of experiment answers to the following questions: 1) What is the cross section for diffractive dissociation? 2) Which part of the cross section scales? 3) What is the shape of the low M_X^2 peak? Many such empirical questions can be properly answered only in conjunction with a complete theory of high energy interactions. In the absence of a complete theory, a certain language has developed amongst the cognoscenti. "Diffractive dissociation" is currently taken to mean that

part of the cross section which is independent of energy and has "low" M_X^2. Such a nebulous definition yields the following queries: a) How low is "low" M^2? b) Are the "low" M_X^2 events also produced by processes which scale with energy? (Namely processes where $sd^2\sigma/dtdM_X^2$ is a constant instead of $d^2\sigma/dtdM_X^2$). We note therefore that questions 1 and 3 are interrelated.

We feel that with the sharp resolution of our spectrometer we can make some unambiguous determinations. We reason as follows: For $M_X^2 > 16$ GeV^2, the cross section is flat in M_X^2. Our value of the cross section for these "large" M_X^2 agree with the determinations from similar experiments performed at NAL[16,17] and ISR[13], after adjusting for the different t regions covered by the experiments, and assuming scaling. We have also taken some lower statistics data at 200 and 400 GeV; the mass spectra were similar to our 300 GeV data and the "large" M_X^2 regions were consistent with scaling. We therefore conclude that diffraction only appears for $M_X^2 <$ 16 GeV^2. The total cross section at these "low" M_X^2, integrating over all t's, is 2.35 $\pm$ 0.2 mb. However, some of this cross section is due to the same physical process which gave rise to the scaling part of the cross section and should be subtracted. A lower bound is obtained by assuming the scaling contribution extends all the way to $M_X^2 = 1$. In this way, we obtain a cross section of 1.6 $\pm$ 0.2 mb. Doubling this value to properly account for the symmetry of the proton-proton system, we obtain $3.2 < \sigma_{diff} < 4.7$ mb.

In seeking an answer to question 3, we have tried to fit our M_X^2 spectrum with various shapes (i.e., with polynomials in $1/M_X$). We come to the conclusion that the "low" mass region does not follow a $1/M_X^2$ dependence. A more reasonable fit is obtained by including a $1/M_X^3$ term. The curve drawn in Fig. 2a corresponds approximately to the following form

$$s[f(M_X^2, \langle t\rangle = -0.1)] = 1.43\ s/M_X^2 + 5.48\ s/M_X^3 + 51 \quad .$$

In fact, we have fitted our data to the triple regge formula

$$s d^2\sigma/dt dM^2 = (m_p^2/s)[\sum_{ijk} G_{ijk}(s/M_X^2)^{\alpha_i(t)+\alpha_j(t)} (M_X^2/m_p^2)^{\alpha_K(o)}]$$

at $\langle t\rangle = -0.1$ where $\alpha_P(t) = 1 + 0.28\ t$, $\alpha_R(t) = 0.5 + t$, and ijk = PPP, PPR, RRP obtaining $G_{PPP} = 1.43\ \frac{mb}{GeV^2}$, $G_{PPR} = 5.48\ \frac{mb}{GeV^2}$, and $G_{RRP} = 51\ \frac{mb}{GeV^2}$. Note that fitting with only three terms is an oversimplification even in the triple regge scheme,[18] and that the fit clearly misses the data points whenever structure occurs. It is amusing to note, however, that the region $8 < M_X^2 < 14\ GeV^2$ is where the $1/M_X^2$ term gives its largest relative contribution to the cross section. It is therefore reasonable to ascribe to this term the particular behavior in t observed in the same mass region. If one, in addition, tries to isolate the particular t dependence of the $1/M_X^2$ term, this can be obtained approximately by subtracting from each other the two spectra shown in Fig. 3 (assuming a straight line spectrum for the high mass region). The result of such a subtraction gives a cross section which vanishes at t = 0 and approximately behaves in t as $|t|e^{12t}$.

ACKNOWLEDGMENTS

We wish to express our thanks to the NAL Accelerator, beam extraction and Neutrino Lab staffs. In particular, we wish to thank J.R. Orr, E. Bleser, and H. Edwards. The Nevis machine shop constructed most of our mechanical equipment and some parts of the electronics were built at Nevis Labs. We gratefully acknowledge the help of W. Sippach and Y. Au. We thank R. McGrath who determined the purity of our polyethene target at the Stony Brook Van de Graaf. We wish to thank our theoretical colleagues, particularly, C. Quigg and A. Mueller, for their continuous encouragement and interest in our experiment. We also thank Paula and Catfish.

REFERENCES

1 U. Amaldi et al, Phys. Letters 44B, 112 (1973).

2 G. Bellettini et al, Phys. Letters 44B, 119 (1973).

3 U. Amaldi, presentation at the Fifth International Conference on High Energy Collisions, Stony Brook (1973).

4 M.L. Good, W.D. Walker, Phys. Rev. 120, 1857 (1960).

5 R.P. Feynman, Phys. Rev. Letters 23, 1415 (1969).

6 A.H. Mueller, Phys. Rev. D2, 2963 (1970).

7 H.D.I. Abarbanel et al, Phys. Rev. Letters 26, 937 (1971).

8 O. Kancheli, Pisma Zh. Eksp. Teor. Fiz. 11, 397 (1970) (JETP Letters 11, 267 (1970)).

R.D. Peccei, A. Pignotti, Phys. Rev. Letters 26, 1076 (1971).

C.E. DeTar et al, Phys. Rev. Letters 26, 675 (1971).

9 R. McCarthy et al, Experiments on High Energy Particle Collisions, Vanderbilt Conference (1973).

R. Schamberger et al, Contribution to the 1973 Meeting of the APS Division of Particles and Fields, Berkeley, (1973).

S. Childress et al, Contribution to the 1973 Meeting of the APS Division of Particles and Fields, Berkeley, (1973).

10 P. Franzini, R. Schamberger, Contribution to the 1973 International Conference on High Energy Collisions, Frascati, Italy.

P. Franzini et al, Contribution to the 1973 International Conference on High Energy Instrumentation, Frascati, Italy.

11 J. Lee-Franzini et al, Contribution to the 1973 International Conference on High Energy Instrumentation, Frascati.

[12] Barbiellini et al, Phys. Letters 39B, 663 (1972).

[13] M.G. Albrow et al, Nucl. Phys. B54, 6 (1973).

M.G. Albrow et al, Nucl. Phys. B51, 388 (1973).

[14] E.W. Anderson et al, Phys. Rev. Letters 19, 198 (1967).

R.M. Edelstein et al, Phys. Rev. D5, 1073 (1972).

J.V. Allaby et al, Nucl. Phys. B52, 316 (1973).

[15] R. Cool et al, Contribution to the 1973 Meeting of the APS Division of Particles and Fields, Berkeley, (1973).

[16] F. Sannes et al, Contribution to the 1973 Meeting of the APS Division of Particles and Fields, Berkeley, (1973).

[17] J. Van der Velde, Contribution to the Fifth International Conference on High Energy Collisions, Stony Brook, (1973).

[18] S.D. Ellis, A.I. Sanda, Phys. Rev. D6, 1347 (1972).

F.E. Paige, L.L. Wang, Nucl. Phys. B46, 477 (1972).

FIGURE CAPTIONS

Fig. 1a Schematic of solid state detector hodoscope in NAL Neutrino Lab beam line

1b E_1 vs E_2 plot showing particles observed in 300 GeV proton-carbon interactions

Fig. 2a $s \frac{d^2\sigma}{dtdM_X^2}$ vs M_X^2 for $0.019 < |t| < 0.19$ $(GeV/c)^2$; the dashed line has been hand drawn through the data points; for interpretation of the continuous line, see text.

2b $\frac{s}{\pi} \frac{d^2\sigma}{dtdM_X^2}$ vs M_X^2 for $0.019 < |t| < 0.094$ $(GeV/c)^2$; also shown is a comparison with ISR data at $\langle t \rangle = -0.35$.

Fig. 3 $s \frac{d^2\sigma}{dtdM_X^2}$ vs $|t|$, for $8\ GeV^2 \leq M_X^2 \leq 14\ GeV^2$, and $20\ GeV^2 \leq M_X^2 \leq 60\ GeV^2$.

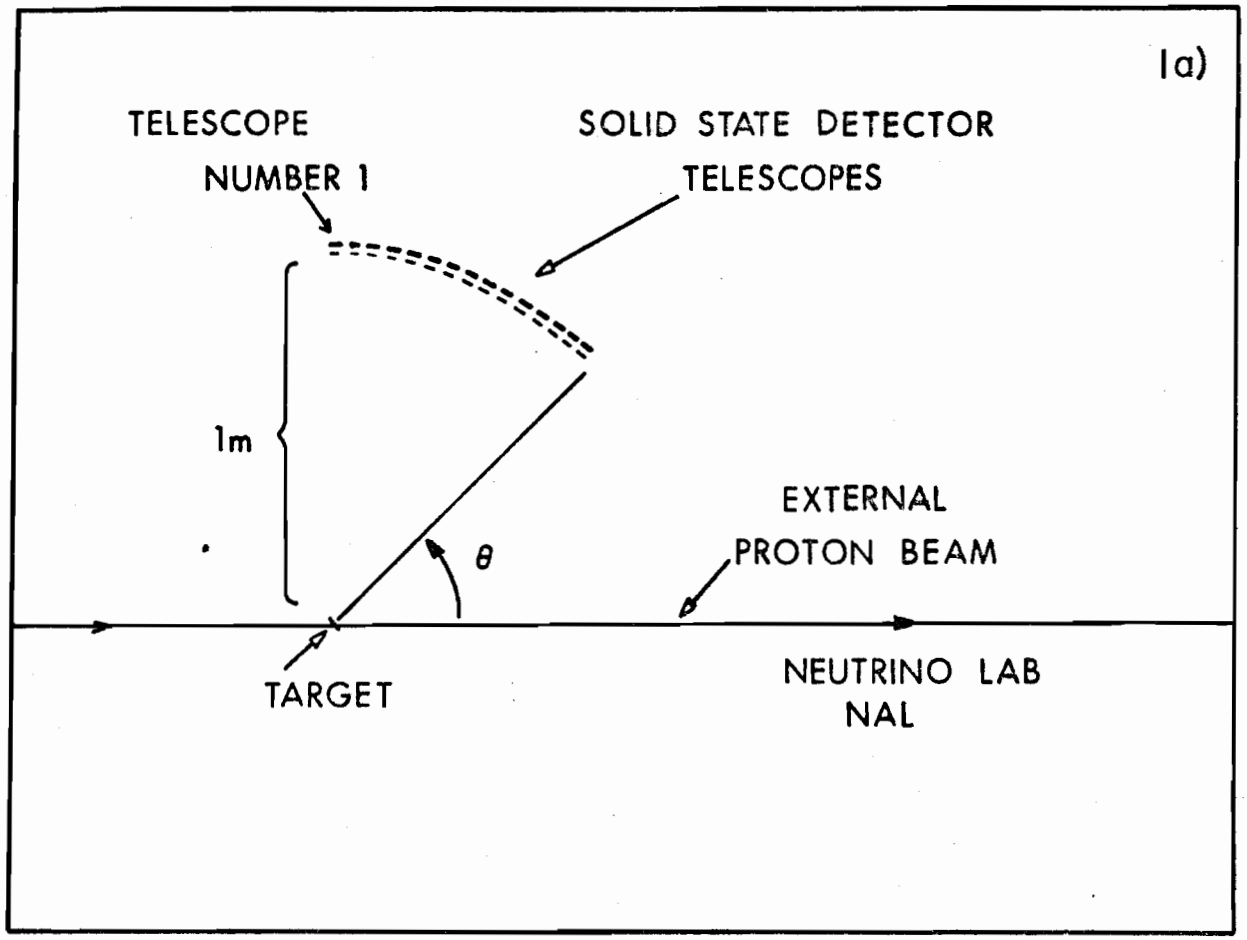
1a)
TELESCOPE
NUMBER 1
SOLID STATE DETECTOR
TELESCOPES
1m
θ
EXTERNAL
PROTON BEAM
TARGET
NEUTRINO LAB
NAL

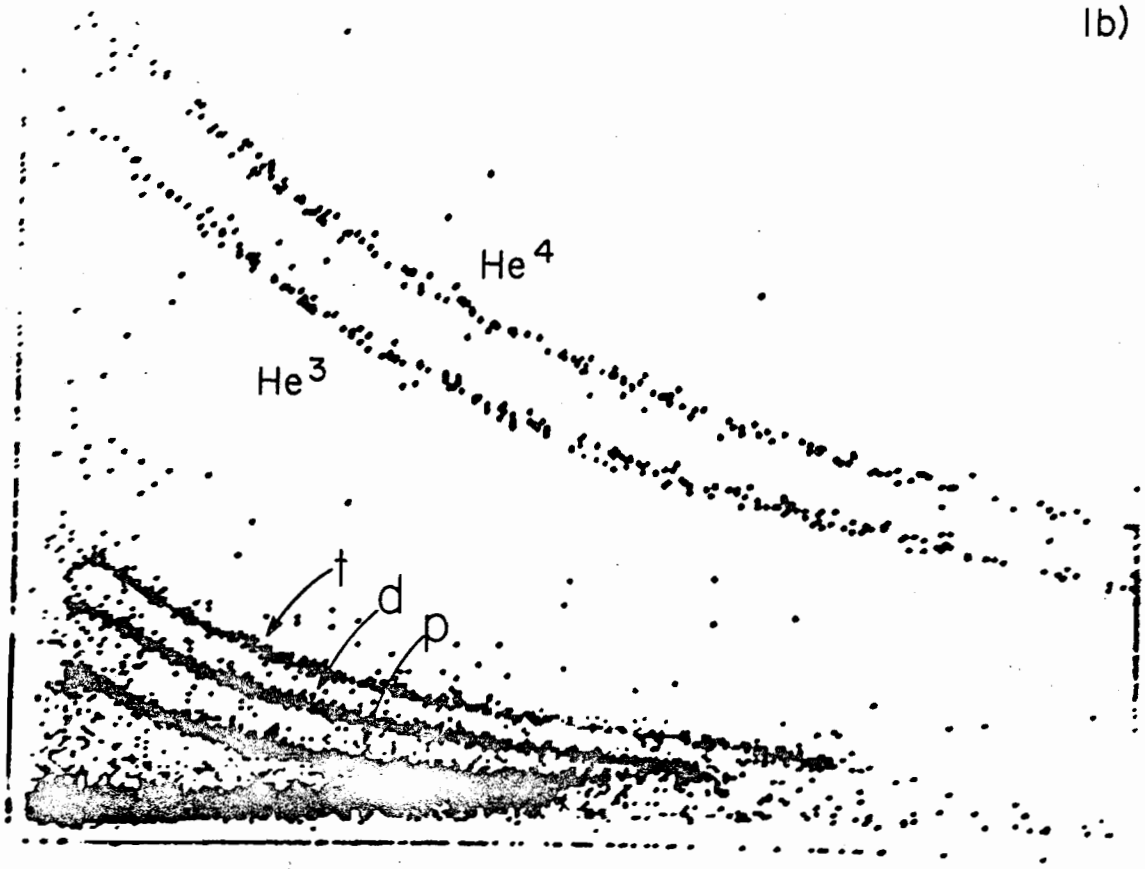
1b)
He4
He3
t
d
p

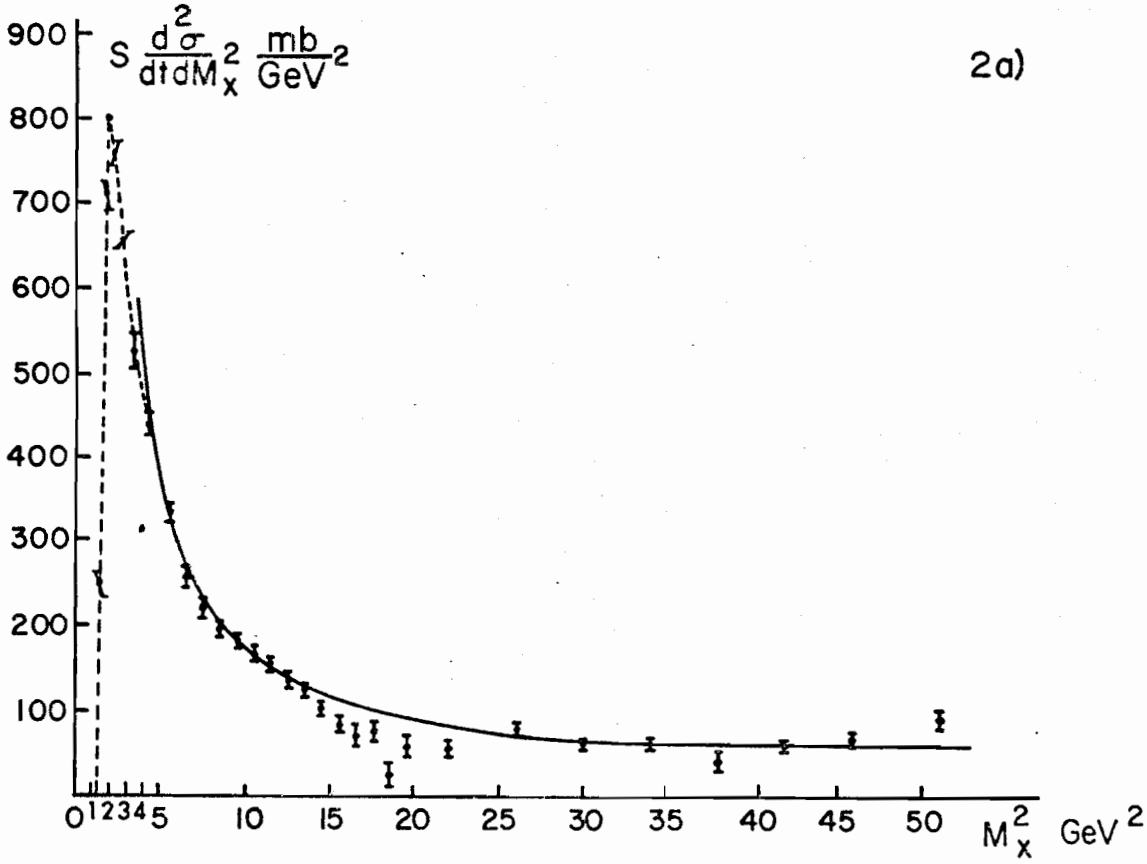
2a)
$S \frac{d^2\sigma}{dt\,dM_x^2} \frac{mb}{GeV^2}$
900
800
700
600
500
400
300
200
100
0 1 2 3 4 5 10 15 20 25 30 35 40 45 50
M_x^2 GeV^2

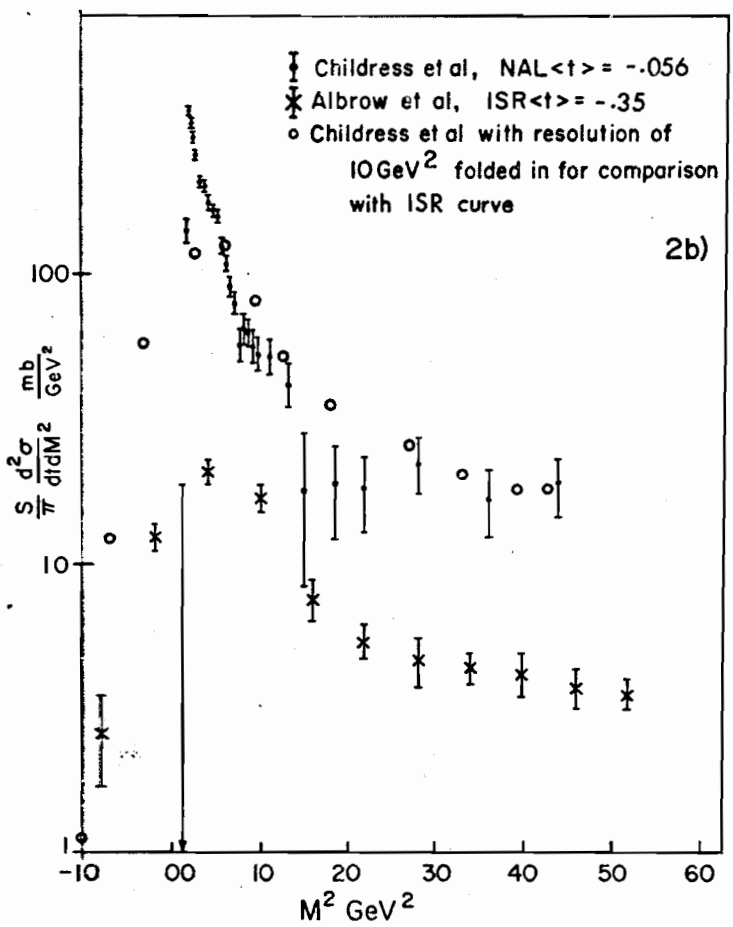
Childress et al, NAL<t> = -.056
Albrow et al, ISR<t> = -.35
Childress et al with resolution of 10 GeV^2 folded in for comparison with ISR curve
2b)
$\frac{S}{\pi} \frac{d^2\sigma}{dt\,dM^2} \frac{mb}{GeV^2}$
100
10
1
-10 00 10 20 30 40 50 60
M^2 GeV^2

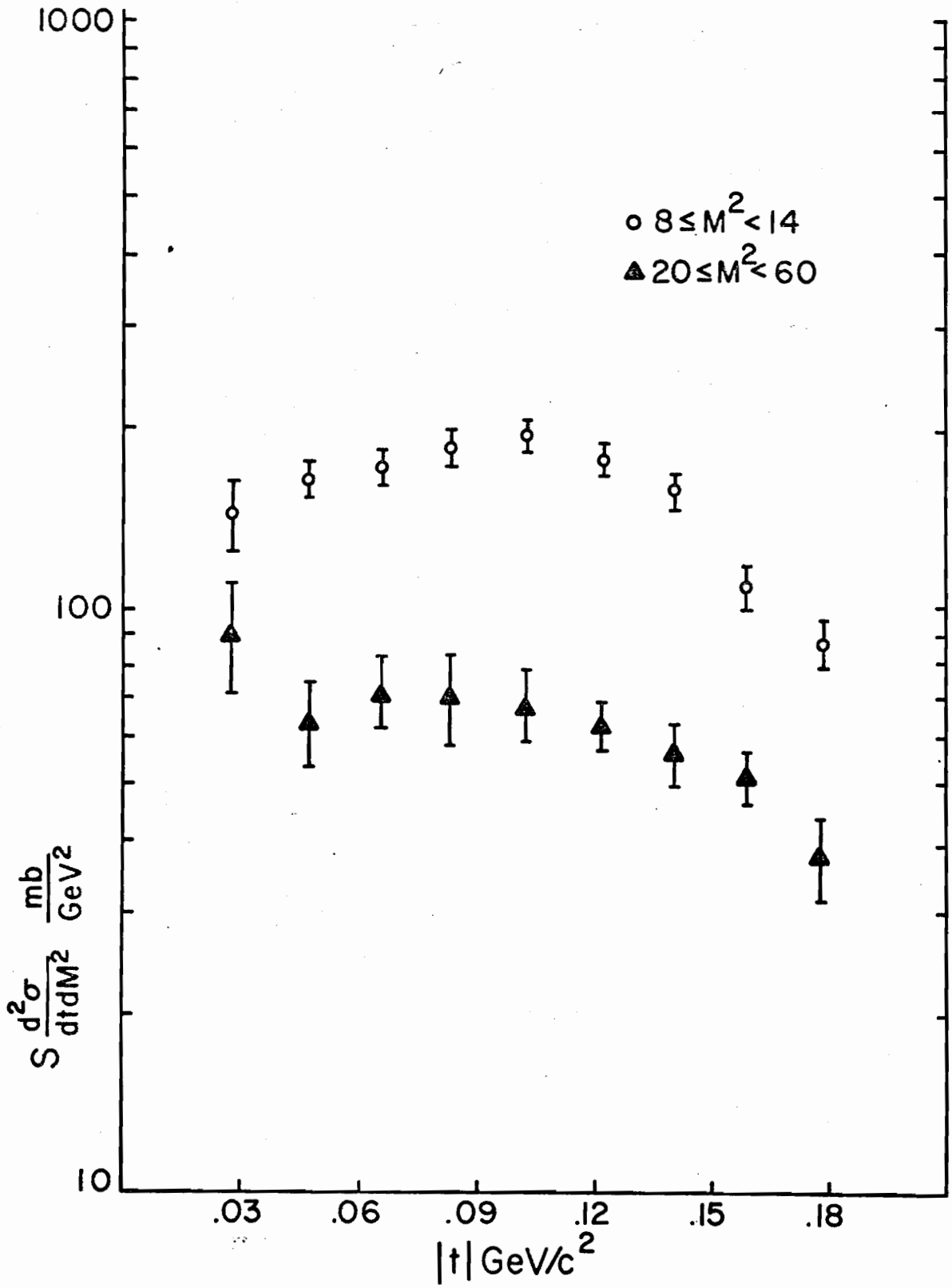
1000
100
10
o 8≤M²<14
▲ 20≤M²<60
S d²σ/dtdM² mb/GeV²
.03
.06
.09
.12
.15
.18
|t| GeV/c²